NANO LETTERS

pubs.acs.org/NanoLett Letter

A Bionic Nano-Band-Aid Constructed by the Three-Stage Self-Assembly of Peptides for Rapid Liver Hemostasis

Jin Yan,*◆ Yang Wang,◆ Xiao Li,◆ Dongnan Guo, Zhengjun Zhou, Ge Bai, Jianhui Li, Na Huang, Jiajie Diao, Yong Li, Wangxiao He,* Wenjia Liu,* and Kaishan Tao*

Cite This: https://doi.org/10.1021/acs.nanolett.1c01800 Read Online

ACCESS | Metrics & More | Article Recommendations | Supporting Information

ABSTRACT: Critical challenges remain in trauma emergency and surgical procedures involving liver bleeding, particularly in perforating wounds that cannot be pressed and large wounds that cannot be sewn. Self-assembling peptide hydrogels are particularly attractive due to their intrinsic biocompatibility and programmability. Herein, we develop a nano-band-aid (NBA) through a three-stage self-assembly strategy of two functionalized peptides, which were first coassembled into nanofibers and then woven to a meshlike network driven by Ca^{2+}. Then, catalyzed by blood coagulation factor XIIIa (FXIIIa), NBA underwent a third stage, self-assembly into a densely compacted physical barrier to stop and control the bleeding. As expected, NBA rapidly and efficiently stopped the bleeding in rat liver scratches while effectively reducing the inflammation around the wound and promoting the wound healing. This bionic self-assembly strategy will provide a clinically potential peptide-based treatment for fatal liver bleeding and reinvigorate efforts to develop self-assembling peptide hydrogels as hemostatic agents.

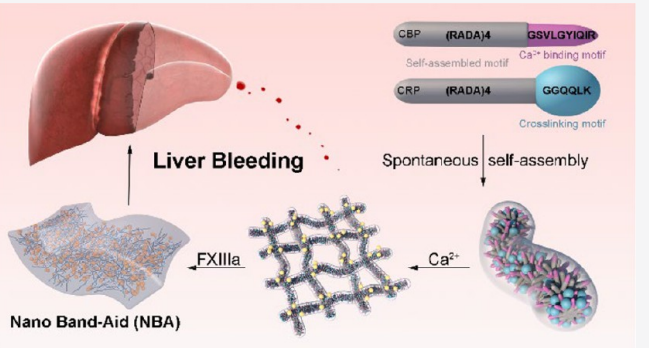

KEYWORDS: *peptide, self-assembly, hemostasis, liver bleeding, peptide supramolecule*

INTRODUCTION

An estimated 5.8 million people die from severe trauma annually around the world, corresponding to almost 16 000 deaths each day.[1] According to statistics from the World Health Organization (WHO), road traffic accidents, suicides, homicides, and warfare are the leading causes of trauma,[2] and in these cases, the liver is the most frequently injured intra-abdominal organ, contributing to at least 10% of the mortalities.[3] Uncontrolled and massive post-traumatic liver bleeding remains a primary and potentially preventable cause of fatalities,[1,4] and even if the rescue is timely, these patients would suffer from life-threatening coagulopathy.[5,6] Whether on the battlefield or in daily rescue, rapid and effective hemostasis is the core principle for a liver trauma emergency. Besides, bleeding inevitably occurs in major liver surgery, including partial liver resection and liver transplantation, which goes against the postoperative effect.[7] Although there have been numerous efforts to deal with and prevent excessive blood loss in liver surgery, hemorrhage as a surgical complication is still a crucial concern in individual patients, particularly those experiencing a large surface resection of liver.[7,8] More importantly, the body's own blood-clotting capability is unable to rapidly stop the bleeding in instances of massive ongoing blood loss.[9] Therefore, the use of hemostatic agents to quickly stop the bleeding from the liver is meaningful for both trauma emergency and surgical procedures involving the liver.

To this end, two broad categories of hemostatic materials have emerged: (1) inorganic materials represented by Combat Gauze, QuikClot, and WoundStat,[10,11] and (2) polymer materials including HemCon and Celox.[12,13] The inorganic materials often promote blood clot formation and catalyze the conversion from fibrinogen to fibrin, resulting in a decent hemostatic effect.[14] The polymer hemostatic materials have always served as a physical barrier for preventing hemorrhage.[15] While many successes have been achieved by these two kinds of materials in hemostasis during trauma emergency and surgical procedures involving the liver, significant challenges remain regarding rapid and efficient control of hemorrhage, especially in perforating wounds that cannot be pressed to stop the blood and large wounds that cannot be sewn.[16] Moreover, commercial hemostatic agents often lead to side effects, including secondary damage from the exothermic

Received: May 8, 2021
Revised: August 26, 2021

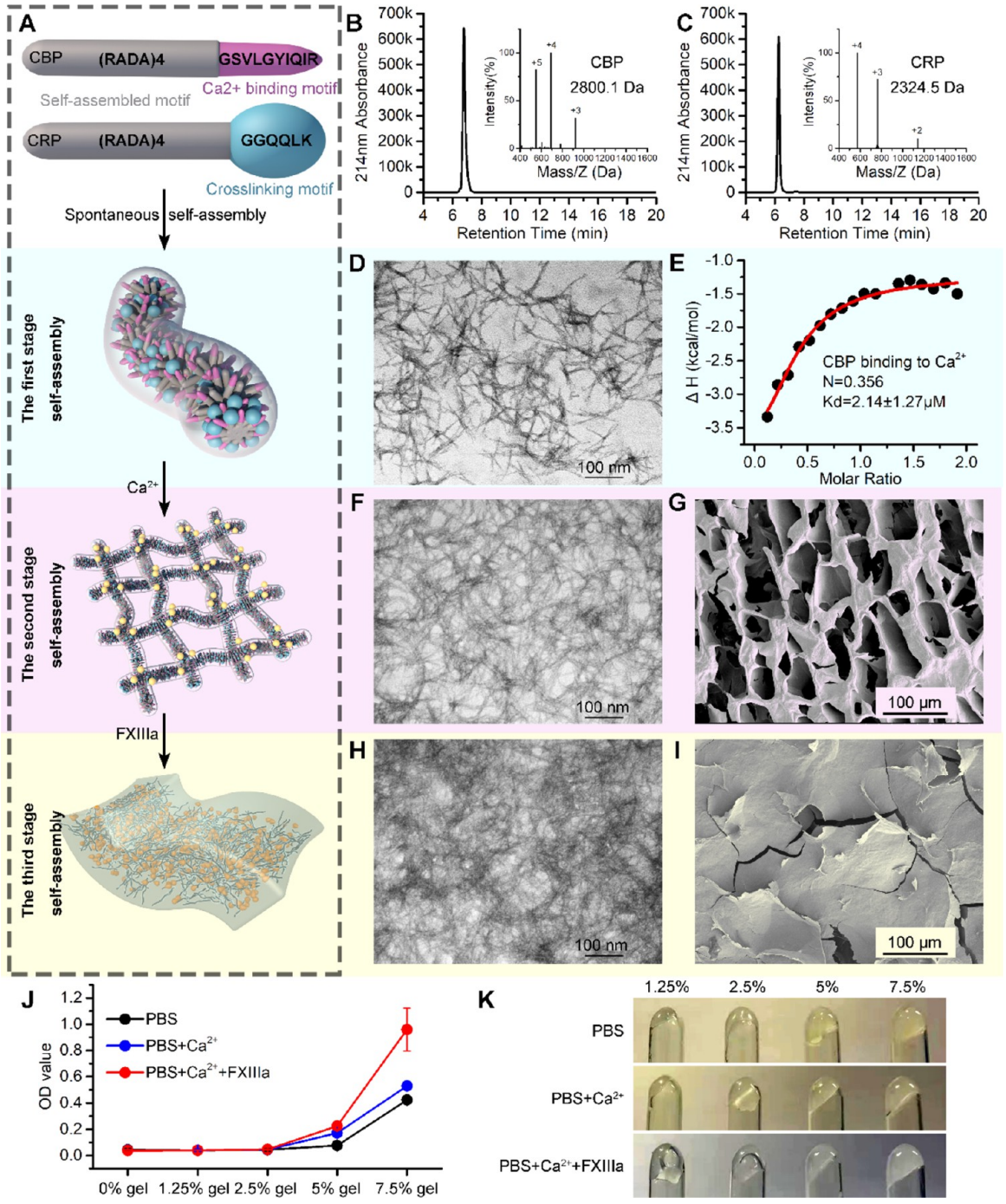

Figure 1. Design and characteristics of NBA. (A) Schematic diagram of three-stage self-assembly strategy of two functionalized peptides, CRP and CBP. (B) and (C) Characterization of synthesized CBP (B) and CRP (C) by LC-MS. (D) TEM image of nanofibers constructed by the first stage of self-assembly of CRP and CBP in PBS buffer. (E) Isothermal titration calorimetry (ITC) assay of the affinity between CBP and Ca^{2+}. The binding affinity was measured at 25 °C in PBS buffer at pH 7.4. (F and G) TEM image (F) and SEM image (G) after the Ca^{2+} driving second stage of self-assembly. (H and I) TEM image (H) and SEM image (I) after the blood coagulation factor XIIIa (FXIIIa) catalyzed the third stage of self-assembly. (J) Gelatinization quantized by the absorbance at 600 nm. (K) Representative photography showing the gelatinization of CRP/CBP peptide hydrogel in response to Ca^{2+} and FXIIIa.

reaction of the inorganic products and biotoxicity from the degradation of polymer products.[17,18] Thus, it is imperative to develop biocompatible hemostatic materials that do not lead to side effects.

To address these issues, self-assembling peptide hydrogels are particularly attractive as hemostatic materials because of their intrinsic biocompatibility and safety.[19,20] Driven by noncovalent weak interaction such as hydrophobic interaction, electrostatic interactions, and hydrogen-bonding, self-assembling peptides including SPG-178,[21] EAK16,[22] SLac,[23] and RADA16,[24] can gel at bleeding sites, significantly reducing blood loss.[25] However, this self-assembly driven by weak interaction is both a 4O08blessing and a curse; being capable of self-assembly into specific network nanostructures was a paramount benefit of these peptides, but the weak intermolecular interaction made them fragile and unsuited

https://doi.org/10.1021/acs.nanolett.1c01800
Nano Lett. XXXX, XXX, XXX−XXX

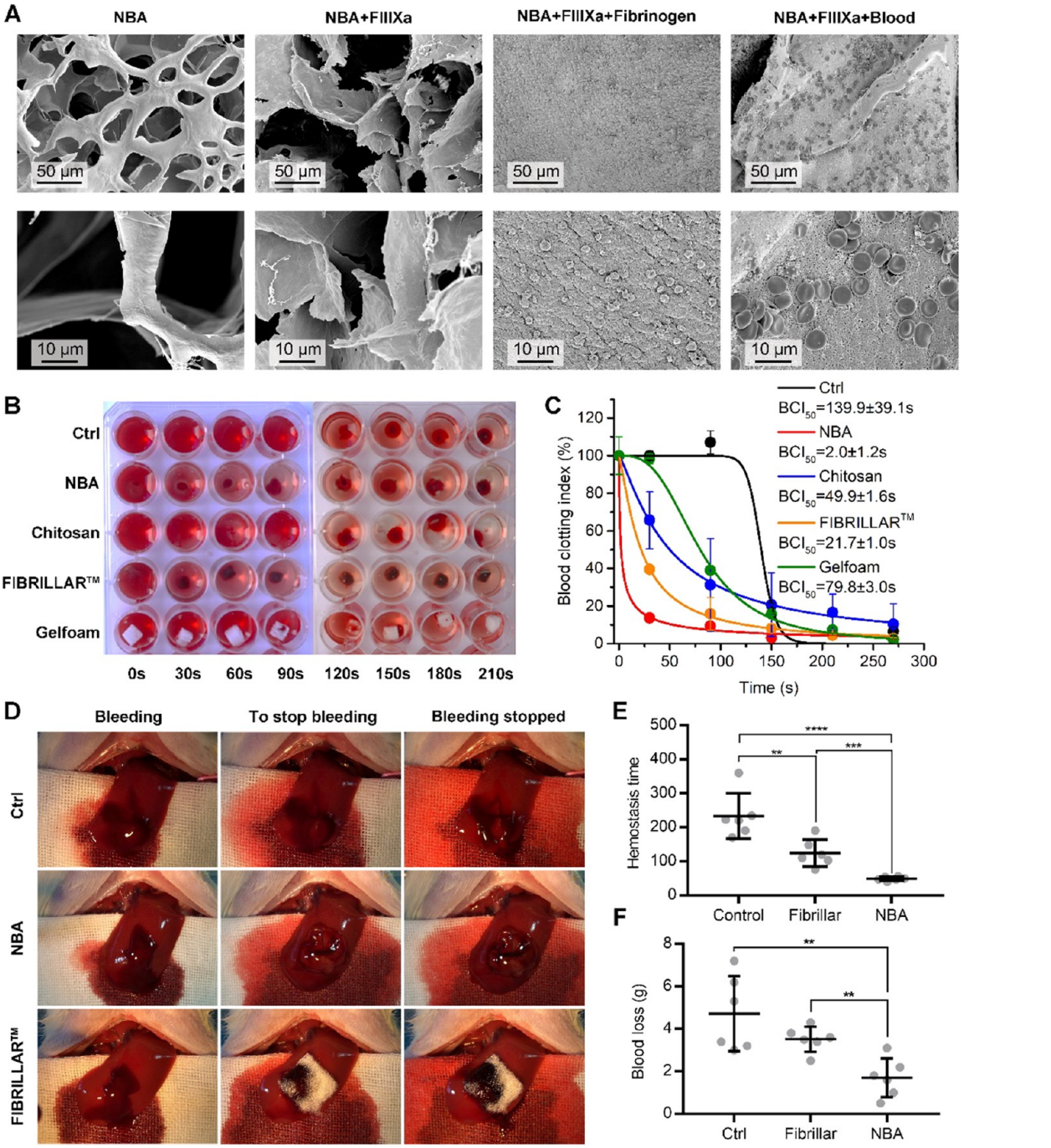

Figure 2. Biofunction of NBA. (A) SEM image of NBA in response to FXIIIa, fibrinogen, and blood, suggesting that NBA has a great potential to weave a compact physical barrier compounded from peptides and fibrins. (B) Representative photography showing the whole-blood-clotting evaluation of the NBA and controls. (C) In vitro dynamic whole-blood-clotting evaluation of the NBA and controls. The absorbance values of blood solutions were measured at 600 nm and the half blood-clotting time (BCI_{50}) were fitted by the logarithmic equation in each group. (D) Representative pictures demonstrating hemostasis in rat liver after the creation of a cut wound with 1 cm long and 0.5 cm depth sagittal. (E) and (F) Hemostatic time (E) and blood loss (F) in the rat liver scratches model (Mean ± SD, $n = 6$/group). p values were calculated by ANOVA. *, $p < 0.05$; **, $p < 0.01$; ***, $p < 0.001$; and ****, $p < 0.0001$.

for blocking the bleeding from arterial blood vessel with high pressure, such as the hepatic artery.[26] Hence, it remains a challenge to develop peptide-derived hemostatic materials with controlled mechanical properties to rapidly and efficiently stop the massive ongoing bleeding.

Herein, to develop a peptide-derived hemostatic material aimed at treating a perforating wound that cannot be pressed and a large wound cannot be sewn, a three-stage self-assembly strategy was designed. In this case, two tailor-designed peptides $(RADA)_4$-GGQQLK (cross-linking peptide, CRP) and $(RADA)_4$-GSVLGYIQIR (Ca^{2+} binding peptide, CBP) were synthesized productively and efficiently by FMOC chemistry (Figure 1A).[27−32] The $(RADA)_4$ peptide possesses the ability of self-assemble into interwoven nanofibers.[20] In the first stage of self-assembly, $(RADA)_4$ motif can endow CRP and CBP with a capacity to coassemble into nanofibers.[20] The functional

https://doi.org/10.1021/acs.nanolett.1c01800
Nano Lett. XXXX, XXX, XXX−XXX

motif VLGYIQIR in CBP flanking around the self-assembling nanofibers is capable of binding to Ca^{2+} with the coordination number 3,[33] driving the second stage of self-assembly into a meshlike network, termed a nano-band-aid (NBA) (Figure 1A). As for the third stage of self-assembly, the other motif flanking (QQLK in CRP) around the nanofibers can be further cross-linked with each other and fibrin via acyl transfer reaction that is catalyzed by blood coagulation factor XIIIa (FXIIIa) in the coagulation cascade (Figure 1A).[34] As a result, when NBA meets blood, it can weave a physical barrier in situ, consisting of peptides and fibrins at bleeding sites. More importantly, this NBA is a viscous fluid before meeting the blood, thereby being propitious for the perforating wound and the large wound. As expected, NBA rapidly and efficiently controls the bleeding in rat liver scratches and penetrating wounds in the non-compressible hemorrhage model and the rat liver defect in the lethal unsuturable hemorrhage model while maintaining a favorable safety property. This bionic three-stage self-assembly strategy will provide a clinically potential peptide-based treatment for fatal liver bleeding and reinvigorate efforts to develop self-assembling peptide hydrogels as hemostatics with a wide range of potential applications.

RESULTS AND DISCUSSION

CRP and CBP were synthesized by solid-phase peptide synthesis (SPPS) following the FMOC chemistry;[35−38] subsequently, they were purified by preparative high-performance liquid chromatography (HPLC) and collected after lyophilization. As shown in Figure 1B,C, the two peptides were successfully synthesized as identified by liquid chromatography−mass spectrometry (LC-MS) analysis, in which the molecular weights are correct, and their purity exceeded 95%. Notably, the productivity of both CRP and CBP was greater than 75%, promoting its application potential. Dissolving CRP and CBP in PBS buffer (pH 7.4) triggered the first stage of self-assembly into sparsely wired nanofibers as evidenced by the transmission electron microscope (TEM) image (Figure 1D). Besides, as designed, CBP has a function for binding calcium ions, which was the driving force of the secondary self-assembly. Measuring by isothermal titration calorimetry analysis, CBP binds to Ca^{2+} with a high affinity of 2.14 μM and site number of 0.356 (Figure 1E), suggesting that CBP can be efficiently conjugated with 3 calcium ions. As a result, this feature induced the cross-linking among nanofibers, organizing into a meshlike network, or NBA (Figure 1F,G). To optimize this network structure, we screened the ratio of CBP to CRP. As shown in the scanning electron microscopy (SEM) image in Figure S1, the optimal ratio of 3:1 (CBP/CRP) is most conducive to the conformation of this meshlike network (Figure S1). Notably, the TEM image combined with in situ Ca elemental analysis further supported this result, in which Ca can be found in the crossing of nanofibers (Figure S2).

Moreover, the further cross-linking between the QQLK motifs in CRP would drive the third stage of self-assembly. As expected, FXIIIa can catalyze this reaction and weave the meshlike network into more densely compacted nanofibrous entanglements (Figure 1H,I). In addition, this three-stage self-assembly of peptides was proved again by the gelation analysis, where the highest absorbance at 600 nm corresponding to the densest gel was shown in the condition containing Ca^{2+} and FXIIIa, in sharp contrast to the lowest absorbance with the peptide-only condition (Figure 1J,K). However, a hydrogel was not formed when mixing $(RADA)_4$, GSVLGYIQIR, and GGQQLK peptides, even under the condition of Ca^{2+} and FXIIIa (Figure S3) as supported by the image (Figure S3A), absorbence (Figure S3B), and rheological properties (Figure S3C). Notably, 5% peptide density is a critical concentration at which NBA maintained fluidity before FXIIIa catalysis and completely transferred to solid gel after catalysis (Figure 1K). Thus, this concentration was used for subsequent functional test. To test the mechanical properties of the NBA, the rheological measurements and atomic force microscopy (AFM) analysis were used to measure the resilience and stiffness at a density of 5% NBA. As shown in Figure S4, the storage modulus (G') of the NBA hydrogel ranged from 0.03 to 0.22 Pa (Figure S4A), while the dissipated energy (G'') ranged from 0.02 to 0.08 Pa (Figure S4A). Notably, a 7-fold enhancement in the rheological stiffness of NBA can be found after they were cross-linked with Ca^{2+} and blood coagulation factor XIIIa (FXIIIa). Besides, both rheometer and AFM measured tangent values of the loss angle ($\tan \delta$) of NBA were less than 1 (Figure S4C and Table S1), which indicated it was a viscoelastic solid. In addition, the decrease of the $\tan \delta$ value indicated that NBA gained more resilience after it was cross-linked with Ca^{2+} and FXIIIa (Figure S4C and Table S1).

Before the functional test, we first explored the in vitro acute toxicity of NBA by measuring the viability of hepatocyte (AML12 cell line) and vascular endothelial cells (HUVEC cell line) after incubation with NBA. As shown in Figure S7, no cytotoxicity can be found during 7 days of incubation, suggesting the safety and biocompatibility of NBA. Next, to explore the biofunction of NBA, SEM was used to observe the microstructural change of NBA after incubation with fibrinogen and blood upon the presence of FXIIIa. As shown in Figure 2A, fibrinogen further increased the compactness of NBA, presumably because of the FXIIIa-catalyzed co-cross-linking between fibrinogen and NBA. Moreover, the increased compactness can also be found after the coincubation of NBA with FXIIIa and blood (Figure 2A). Once the compact physical barrier was formed, the red blood cells, with a diameter of about 7 μm, and some larger structures in blood have difficulty entering the inside of the NBA structure, which further strengthens hemostasis. These results demonstrated that NBA has a great potential to weave a compact physical barrier in situ at bleeding sites compounded from peptides and fibrins.

Next, we evaluated the in vitro blood-clotting performance of NBA by dynamic whole-blood-clotting test.[16] For comparative study, equiponderant commercial gelatin hemostatic sponge (Gelfoam), chitosan blood stop powder (chitosan), and hemostatic fiber yarn (Fibrillar) were used as the positive controls. In this test, a lower transmittance of the hemoglobin solution indicates a higher clotting rate. As shown, both NBA and Fibrillar resulted in the clarity after 60s incubation with blood, indicative of their outstanding blood-clotting performance (Figure 2B). To quantify their blood-clotting capability, the absorbance values of blood solutions were measured at 600 nm, and the half blood-clotting time (BCI_{50}) was fitted by the logarithmic equation in each group. As shown in Figure 2C, NBA, Gelfoam, chitosan, and Fibrillar significantly shortened the half blood-clotting time of blood. Importantly, NBA had the shortest BCI_{50} values of an amazing 2.0 s, and Fibrillar had sublevel blood-clotting capability with BCI_{50} of 21.7s. Thus, Fibrillar was chosen as the positive control in the in vivo test.

The hemostatic property of NBA was further evaluated in a serious rat liver injury model, for which two crossed 1 cm long

https://doi.org/10.1021/acs.nanolett.1c01800
Nano Lett. XXXX, XXX, XXX−XXX

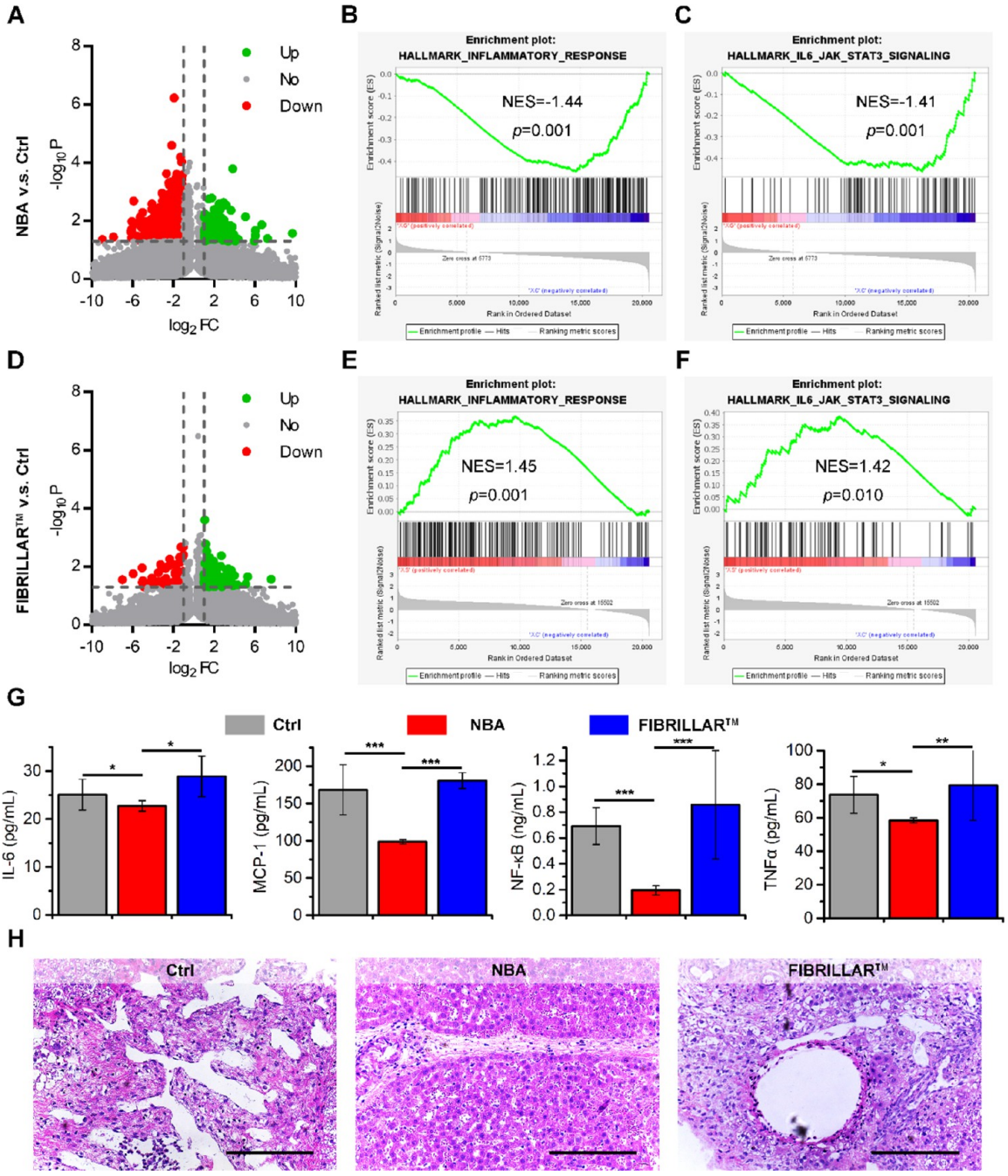

Figure 3. NBA effectively reduced the inflammation around the wound and promoted wound healing. (A) Volcano plot of genes differentially expressed in wound tissue after NBA treatment compared to PBS treatment (n = 3). (B) and (C) Gene set enrichment analysis (GSEA) results for inflammatory response (B) and IL6-JAK-STAT3 signaling pathway (C) in response to NBA treatment. (D) Volcano plot of genes differentially expressed in wound tissue after FIBRILLAR treatment compared to PBS treatment (n = 3). (E and F) GSEA results for inflammatory response (E) and IL6-JAK-STAT3 signaling pathway (F) in response to FIBRILLAR treatment. (G) the ELISA assay to quantify four inflammatory factors in wound tissue: IL-6, MCP-1, NF-κB, and TNFα. (H) Representative H&E image of the wound in the liver 14 days after the indicated treatment.

and 0.5 cm deep sagittal incisions were created to simulate a serious wound that cannot be sewn, and the experimental procedure was approved by the medical ethics committee of The Fourth Military Medical University. As shown in Figure 2D, this severe liver injury resulted in quick and profuse bleeding, and 5% NBA or equiponderant Fibrillar was used to treated these wounds at 15 s postbleeding. As expected, in NBA-treated liver, the hydrogel rapidly conformed to the lesion and immediately gelated in situ (Movie S1). More importantly, NBA achieved hemostasis in less than 50 s in contrast to the 120 s necessary for Fibrillar, whereas it took more than 220 s for the bleeding in the control group to totally stop (Figure 2E). In addition, NBA statistically significantly reduced blood loss in comparison to the Fibrillar and PBS-treated group (Ctrl) (Figure 2F). Moreover, after hemostasis, the hydrogel can stay on the surface of the liver for more than 3 min when placed vertically (Figure S5), which suggested good tissue adhesiveness. These results demonstrated the excellent in vivo hemostatic capacity of NBA.

https://doi.org/10.1021/acs.nanolett.1c01800
Nano Lett. XXXX, XXX, XXX−XXX

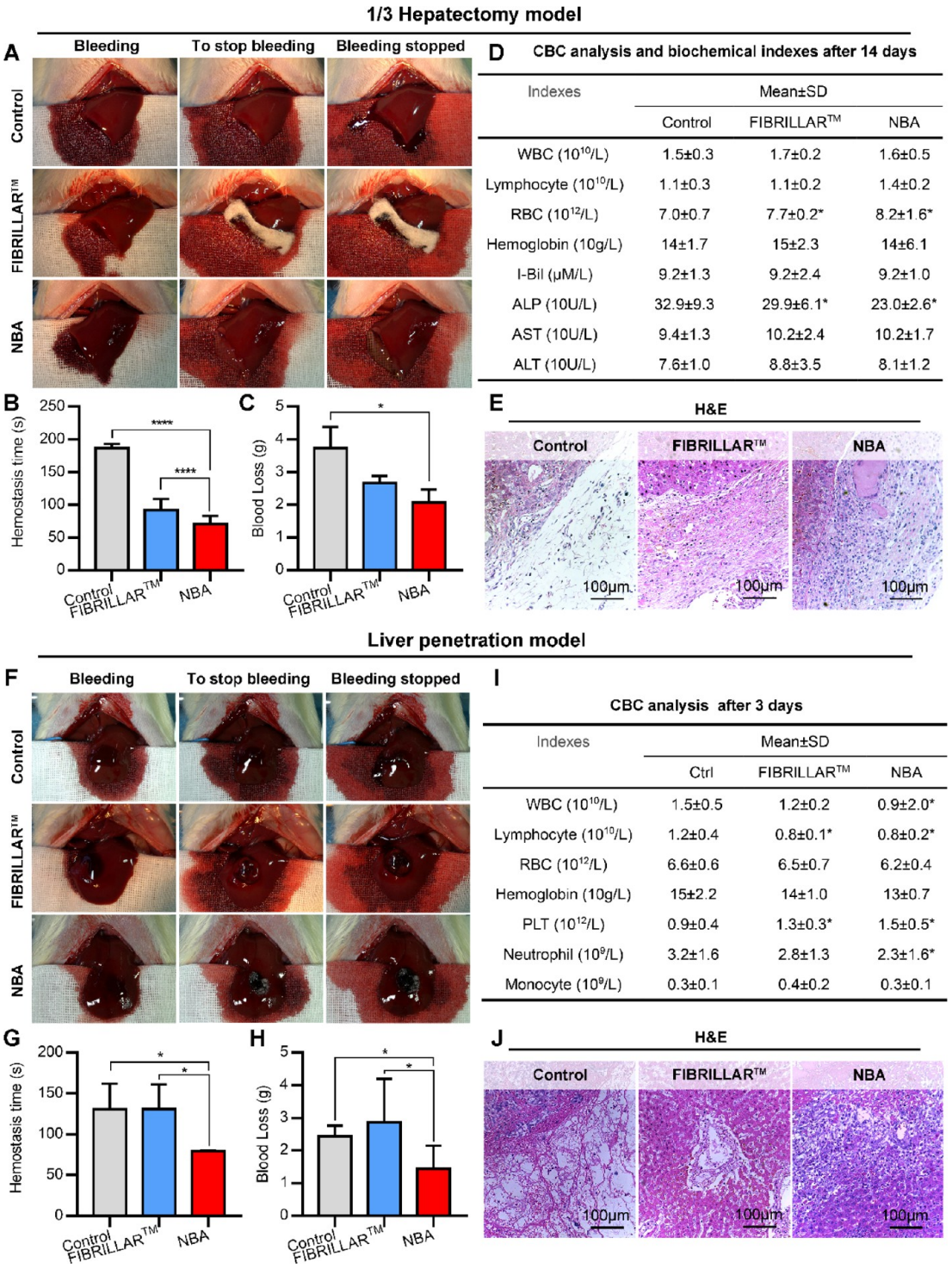

Indexes	Mean±SD		
	Control	FIBRILLAR™	NBA
WBC (10^{10}/L)	1.5±0.3	1.7±0.2	1.6±0.5
Lymphocyte (10^{10}/L)	1.1±0.3	1.1±0.2	1.4±0.2
RBC (10^{12}/L)	7.0±0.7	7.7±0.2*	8.2±1.6*
Hemoglobin (10g/L)	14±1.7	15±2.3	14±6.1
I-Bil (μM/L)	9.2±1.3	9.2±2.4	9.2±1.0
ALP (10U/L)	32.9±9.3	29.9±6.1*	23.0±2.6*
AST (10U/L)	9.4±1.3	10.2±2.4	10.2±1.7
ALT (10U/L)	7.6±1.0	8.8±3.5	8.1±1.2

Indexes	Mean±SD		
	Ctrl	FIBRILLAR™	NBA
WBC (10^{10}/L)	1.5±0.5	1.2±0.2	0.9±2.0*
Lymphocyte (10^{10}/L)	1.2±0.4	0.8±0.1*	0.8±0.2*
RBC (10^{12}/L)	6.6±0.6	6.5±0.7	6.2±0.4
Hemoglobin (10g/L)	15±2.2	14±1.0	13±0.7
PLT (10^{12}/L)	0.9±0.4	1.3±0.3*	1.5±0.5*
Neutrophil (10^{9}/L)	3.2±1.6	2.8±1.3	2.3±1.6*
Monocyte (10^{9}/L)	0.3±0.1	0.4±0.2	0.3±0.1

Figure 4. NBA presented excellent hemostatic effects on a rat liver defect: lethal, unsuturable hemorrhage model and a penetrating wound, noncompressible hemorrhage model. (A) Representative pictures demonstrating hemostasis in rat liver after the creation of a rat liver $^{1}/_{3}$ defect lethal unsuturable hemorrhage model. (B and C) Hemostatic time (B) and blood loss (C) in the rat liver scratches model (mean ± SD, n = 6/group). (D) Complete blood cell count and hepatic biochemistry measurement at 14 days after the indicated treatment. (E) Representative H&E image of the wound in the liver at 14 days after the indicated treatment. (F) Representative pictures demonstrating hemostasis in rat liver after the creation of a penetrating wound, noncompressible hemorrhage model. (G and H) Hemostatic time (G) and blood loss (H) in the rat liver scratches model (mean ± SD, n = 6/group). (I) Complete blood cell counts at 3 days after the indicated treatment. (J) Representative H&E image of the wound in the liver at 14 days after the indicated treatment. The p values were calculated by ANOVA. *, $p < 0.05$; **, $p < 0.01$; ***, $p < 0.001$; and ****, $p < 0.0001$.

On account of the rapid hemostatic ability and excellent biocompatibility, we hypothesized that NBA can effectively reduce the inflammation around the wound, which is highly conducive to the wound healing. To verify it, 1 cm^3 wound tissue was isolated from the injured liver 3 days after hemostatic therapy. Analysis by RNA sequencing showed

https://doi.org/10.1021/acs.nanolett.1c01800
Nano Lett. XXXX, XXX, XXX−XXX

that NBA triggered 920 differential changes in gene expression compared to PBS control (Figure 3A), and a consistent and reproducible enrichment of inflammatory-regulated gene expression signatures can be found by gene set enrichment analysis (GSEA) (Figure 3B,C). In detail, NBA resulted in a statistically significant downregulation in the pathway of inflammatory response (Figure 3B) and IL6-JAK-STAT3 signaling (Figure 3C). In sharp contrast, comparing Fibrillar with PBS control, although we found just 162 differentially expressed genes (Figure 3D), Fibrillar statistically significantly upregulated the inflammatory response (Figure 3E) and IL6-JAK-STAT3 signaling pathway (Figure 3F), presumably because of its limited biocompatibility. To further validate these results, we performed the enzyme-linked immunosorbent assay (ELISA) to quantify four inflammatory factors in wound tissue, IL-6, MCP-1, NF-κB, and TNFα, and these results again validated that NBA can effectively reduce the inflammation (Figure 3G).

Besides, NBA treatment promoted wound healing as evidenced by the hepatic pathology section and the surface recovery of the wound at 14 days post-treatment (Figures 3H and S6). These results were further supported by the normalized hepatic function indexes (Tables S2 and S3) and complete blood counts (Table S4). Furthermore, no pathological change can be found in the heart, spleen, lung, and kidney of mice after NBA treatment (Figure S8), supporting the safety of NBA. Collectively, NBA has excellent performance in hemostatic treatment and reducing inflammation, showing a huge potential as a rapid, efficient, and safe liver hemostatic material.

To further challenge the hemostatic capacity of NBA, a rat liver defect, lethal unsuturable hemorrhage model and a penetrating wound, noncompressible hemorrhage model were established. As shown in Figure 4A, over $^1/_3$ of the liver was removed (Figure 4A), and more than half the whole blood was lost after the injury (Figure 4B,C). At 15 s after bleeding, compression was performed in the control group, and NBA or Fibrillar were used to treat the wound in the other two groups. As expected, NBA significantly shortened the hemostasis time in comparison to the compression group or the Fibrillar-treated group. Meanwhile, NBA treatment reduced the amount of bleeding by half compared to the compression (Figure 4C). Moreover, NBA also promoted the wound healing and liver function recovery (Figure 4D,E), while maintaining favorable safety properties (Figure S9).

Especially, small and deep penetrating wounds incurred by small-bore weapons and improvised explosive devices are uncompressible, and it is difficult to stop their bleeding by conventional hemostatic agents. As shown in Figure 4F, a 50 mm diameter penetrating wound caused severe bleeding, but Fibrillar presented no hemostatic effect on this massive hemorrhage (Figure 4G,H). In sharp contrast, NBA rapidly flew through the wound and immediately gelated in situ to block the bleeding (Movie S2 and Figure 4F). As a result, NBA treatment cut the time of bleeding in half (Figure 4G) and halved the amount of bleeding (Figure 4H). Besides, 3 days after treatment, the significantly decreased white blood cell (WBC) and neutrophil demonstrated lower inflammation after NBA therapy (Figure 4I). Moreover, NBA also promoted wound healing (Figure 4J).

CONCLUSION

In conclusion, we herein developed a nano-band-aid (NBA) to stop bleeding quickly and efficiently through a three-stage self-assembly strategy of two functionalized peptides. NBA was constructed through a two-stage self-assembly by which CRP and CBP first coassembled into nanofibers and then were woven into a meshlike network driven by Ca^{2+}. NBA is a viscous fluid before meeting blood, thereby making it propitious to cover and conform to both a perforating wound and a large wound. Catalyzed by blood coagulation factor XIIIa (FXIIIa) that activated NBA at the wound, NBA performed the third stage of self-assembly into a densely compacted physical barrier to stop and control the bleeding. As expected, NBA rapidly and efficiently stops the bleeding in rat liver scratches while effectively reducing the inflammation around the wound and promoting wound healing. More importantly, NBA presented excellent hemostatic effects on unsuturable hemorrhage in the rat $^1/_3$ liver defect and the noncompressible hemorrhage due to a penetrating wound and maintained a favorable safety property at the same time. This bionic three-stage self-assembly strategy will provide a clinically potential peptide-based treatment for fatal liver bleeding and reinvigorate efforts to develop self-assembling peptide hydrogels as hemostatics with a wide range of potential applications.

ASSOCIATED CONTENT

Supporting Information

The Supporting Information is available free of charge at https://pubs.acs.org/doi/10.1021/acs.nanolett.1c01800.

Experimental section and figures including the appropriate proportion of peptides, in situ Ca elemental analysis, the gelatinization of (RADA)4, GSVLGYIQIR, and GGQQLK peptides, mechanical properties of NBA, adhesive properties of the NBA hydrogel, the Ability of NBA to repair wounds, and safety and biocompatibility of NBA (PDF)

Movie S1. Movie of stopping bleeding in liver scratches model (MOV)

Movie S2. Movie of stopping bleeding in liver penetration model (MOV)

AUTHOR INFORMATION

Corresponding Authors

Jin Yan − *National & Local Joint Engineering Research Center of Biodiagnosis and Biotherapy, The Second Affiliated Hospital of Xi'an Jiaotong University, Xi'an 710004, PR China; Institute for Stem Cell & Regenerative Medicine, The Second Affiliated Hospital of Xi'an Jiaotong University, Xi'an 710004, China;* orcid.org/0000-0001-6468-6003; Email: yanjin19920602@xjtu.edu.cn

Wangxiao He − *Institute for Stem Cell & Regenerative Medicine, The Second Affiliated Hospital of Xi'an Jiaotong University, Xi'an 710004, China; Department of Talent Highland, The First Affiliated Hospital of Xi'an Jiaotong University, Xi'an 710061, China;* orcid.org/0000-0002-2054-6022; Email: hewangxiao5366@xjtu.edu.cn

Wenjia Liu − *Institute for Stem Cell & Regenerative Medicine, The Second Affiliated Hospital of Xi'an Jiaotong University, Xi'an 710004, China*; Email: wenjialiu@xjtu.edu.cn

Kaishan Tao − *Department of Hepatobiliary Surgery, Xijing Hospital, The Fourth Military Medical University, Xi'an 710032, China*; Email: taokaishan0686@163.com

https://doi.org/10.1021/acs.nanolett.1c01800
Nano Lett. XXXX, XXX, XXX−XXX

Authors

Yang Wang − *Department of Hepatobiliary Surgery, Xijing Hospital, The Fourth Military Medical University, Xi'an 710032, China*

Xiao Li − *Department of Hepatobiliary Surgery, Xijing Hospital, The Fourth Military Medical University, Xi'an 710032, China*

Dongnan Guo − *Department of Hepatobiliary Surgery, Xijing Hospital, The Fourth Military Medical University, Xi'an 710032, China*

Zhengjun Zhou − *Department of Hepatobiliary Surgery, Xijing Hospital, The Fourth Military Medical University, Xi'an 710032, China*

Ge Bai − *Department of Hepatobiliary Surgery, Xijing Hospital, The Fourth Military Medical University, Xi'an 710032, China*

Jianhui Li − *Department of Hepatobiliary Surgery, Xijing Hospital, The Fourth Military Medical University, Xi'an 710032, China*

Na Huang − *Core Research Laboratory, The Second Affiliated Hospital of Xi'an Jiaotong University, Xi'an, Shaanxi 710004, China*

Jiajie Diao − *Department of Cancer Biology, University of Cincinnati College of Medicine, Cincinnati, Ohio 45267, United States;* orcid.org/0000-0003-4288-3203

Yong Li − *Xijing 986 Hospital Department, Fourth Military Medical University, Xi'an 710032, China*

Complete contact information is available at: https://pubs.acs.org/10.1021/acs.nanolett.1c01800

Author Contributions

◆J.Y., Y.W., and X.L. contributed equally to this work.

Notes

The authors declare no competing financial interest.

■ ACKNOWLEDGMENTS

This work was supported by The Thirteen-five-year Program of medical innovation projects (18CXZ014 and AKJ19J001), The Xijing Hospital Disciplines Boosting Project (XJZT19D02, XJZT18D22, and XJZT15D01), National Key R&D Plan (2017YFC1103703), "The Young Talent Support Plan" of Xi'an Jiaotong University (W.H.), Thousand Talents Plan of Shaanxi Province (W.H.), Institutional Science Foundation of The First Affiliated Hospital of Xi'an Jiaotong University (2019QN-01), Postdoctoral innovation talent support program (no. BX20190278), The Project Supported by Natural Science Basic Research Plan in Shaanxi Province of China (program no. 2020JQ-092), the Fundamental Research Funds for the Central Universities (grant no. 1191319101), and the National Natural Science Foundation of China (no. 22007076, 81970566, and 81670593). We thank Instrument Analysis Center of Xi'an Jiaotong University for their assistance with TEM, HRTEM, and SEM analysis. We also appreciate the help of RNA-seq analysis from BioNovoGene (Suzhou) Co., Ltd.

■ REFERENCES

(1) Spahn, D. R.; Bouillon, B.; Cerny, V.; Duranteau, J.; Filipescu, D.; Hunt, B. J.; Komadina, R.; Maegele, M.; Nardi, G.; Riddez, L.; et al. The European guideline on management of major bleeding and coagulopathy following trauma: fifth edition. *Crit. Care* **2019**, *23*, 98.

(2) Tarchouli, M.; Elabsi, M.; Njoumi, N.; Essarghini, M.; Echarrab, M.; Chkoff, M. R. Liver trauma: What current management? *Hepatobiliary Pancreatic Dis. Int.* **2018**, *17*, 39−44.

(3) Naghavi, M.; Abajobir, A. A.; Abbafati, C.; Abbas, K. M.; Abd-Allah, F.; Abera, S. F.; Aboyans, V.; Adetokunboh, O.; Afshin, A.; Agrawal, A.; Ahmadi, A.; Ahmed, M. B.; et al. Global, regional, and national age-sex specific mortality for 264 causes of death, 1980−2016: a systematic analysis for the Global Burden of Disease Study 2016. *Lancet* **2017**, *390*, 1151−1210.

(4) Davenport, R. A.; Guerreiro, M.; Frith, D.; Rourke, C.; Platton, S.; Cohen, M.; Pearse, R.; Thiemermann, C.; Brohi, K. Activated Protein C Drives the Hyperfibrinolysis of Acute Traumatic Coagulopathy. *Anesthesiology* **2017**, *126*, 115−127.

(5) Frith, D.; Goslings, J. C.; Gaarder, C.; Maegele, M.; Cohen, M. J.; Allard, S.; Johansson, P. I.; Stanworth, S.; Thiemermann, C.; Brohi, K. Definition and drivers of acute traumatic coagulopathy: clinical and experimental investigations. *J. Thromb. Haemostasis* **2010**, *8*, 1919−25.

(6) Khan, S.; Davenport, R.; Raza, I.; Glasgow, S.; De'Ath, H. D.; Johansson, P. I.; Curry, N.; Stanworth, S.; Gaarder, C.; Brohi, K. Damage control resuscitation using blood component therapy in standard doses has a limited effect on coagulopathy during trauma hemorrhage. *Intensive Care Med.* **2015**, *41*, 239−247.

(7) Alkozai, E. M.; Lisman, T.; Porte, R. J. Bleeding in Liver Surgery: Prevention and Treatment. *Clin. Liver Dis.* **2009**, *13*, 145−154.

(8) Tranchart, H.; O'Rourke, N.; Van Dam, R.; Gaillard, M.; Lainas, P.; Sugioka, A.; Wakabayashi, G.; Dagher, I. Bleeding control during laparoscopic liver resection: a review of literature. *J. Hepatobiliary Pancreat. Sci.* **2015**, *22*, 371−8.

(9) Chen, J. W.; Cheng, W.; Chen, S. N.; Xu, W. Q.; Lin, J. H.; Liu, H. Q.; Chen, Q. H. Urushiol-functionalized mesoporous silica nanoparticles and their self-assembly into a Janus membrane as a highly efficient hemostatic material. *Nanoscale* **2018**, *10*, 22818−22829.

(10) Littlejohn, L. F.; Devlin, J. J.; Kircher, S. S.; Lueken, R.; Melia, M. R.; Johnson, A. S. Comparison of Celox-A, ChitoFlex, WoundStat, and combat gauze hemostatic agents versus standard gauze dressing in control of hemorrhage in a swine model of penetrating trauma. *Acad. Emerg. Med.* **2011**, *18*, 340−50.

(11) Gegel, B. T.; Austin, P. N.; Johnson, A. D. An Evidence-Based Review of the Use of a Combat Gauze (QuikClot) for Hemorrhage Control. *AANA J.* **2013**, *81*, 453−458.

(12) Devlin, J. J.; Kircher, S.; Kozen, B. G.; Littlejohn, L. F.; Johnson, A. S. Comparison of ChitoFlex®, CELOX, and QuikClot® in Control of Hemorrhage. *J. Emerg. Med.* **2009**, *41*, 237−245.

(13) Kozen, B. G.; Kircher, S. J.; Henao, J.; Godinez, F. S.; Johnson, A. S. An alternative hemostatic dressing: comparison of CELOX, HemCon, and QuikClot. *Acad. Emerg. Med.* **2008**, *15*, 74−81.

(14) Pourshahrestani, S.; Zeimaran, E.; Djordjevic, I.; Kadri, N. A.; Towler, M. R. Inorganic hemostats: The state-of-the-art and recent advances. *Mater. Sci. Eng., C* **2016**, *58*, 1255−1268.

(15) Yang, X.; Liu, W.; Li, N.; Wang, M. S.; Liang, N.; Ullah, I.; Neve, A. L.; Feng, Y.; Chen, H.; Shi, C. C. Design and development of polysaccharide hemostatic materials and their hemostatic mechanism. *Biomater. Sci.* **2017**, *5*, 2357−2368.

(16) Zhao, X.; Guo, B. L.; Wu, H.; Liang, Y. P.; Ma, P. X. Injectable antibacterial conductive nanocomposite cryogels with rapid shape recovery for noncompressible hemorrhage and wound healing. *Nat. Commun.* **2018**, *9*, 2784.

(17) McManus, J.; Hurtado, T.; Pusateri, A.; Knoop, K. J. A case Series Describing Thermal Injury Resulting From Zeolite Use for Hemorrhage Control in Combat Operations. *Prehosp. Emerg. Care* **2007**, *11*, 67−71.

(18) Wright, J. K.; Kalns, J.; Wolf, E. A.; Traweek, F.; Schwarz, S.; Loeffler, C. K.; Snyder, W.; Yantis, L. D., Jr.; Eggers, J. Thermal injury resulting from application of a granular mineral hemostatic agent. *J. Trauma* **2004**, *57*, 224−30.

(19) Ulijn, R. V.; Smith, A. M. Designing peptide based nanomaterials. *Chem. Soc. Rev.* **2008**, *37*, 664−675.

(20) Huang, L.-C.; Wang, H.-C.; Chen, L.-H.; Ho, C.-Y.; Hsieh, P.-H.; Huang, M.-Y.; Wu, H.-C.; Wang, T.-W. Bioinspired Self-assembling Peptide Hydrogel with Proteoglycan-assisted Growth Factor Delivery for Therapeutic Angiogenesis. *Theranostics* **2019**, *9*, 7072−7087.
(21) Komatsu, S.; Nagai, Y.; Naruse, K.; Kimata, Y. The Neutral Self-Assembling Peptide Hydrogel SPG-178 as a Topical Hemostatic Agent. *PLoS One* **2014**, *9*, e102778.
(22) Luo, Z. L.; Wang, S. K.; Zhang, S. G. Fabrication of self-assembling D-form peptide nanofiber scaffold d-EAK16 for rapid hemostasis. *Biomaterials* **2011**, *32*, 2013−2020.
(23) Kumar, V. A.; Wickremasinghe, N. C.; Shi, S. Y.; Hartgerink, J. D. Nanofibrous Snake Venom Hemostat. *ACS Biomater. Sci. Eng.* **2015**, *1*, 1300−1305.
(24) Bagrov, D.; Gazizova, Y.; Podgorsky, V.; Udovichenko, I.; Danilkovich, A.; Prusakov, K.; Klinov, D. Morphology and Aggregation of RADA-16-I Peptide Studied by AFM, NMR and Molecular Dynamics Simulations. *Biopolymers* **2016**, *106*, 72−81.
(25) Hao, R. R.; Peng, X. T.; Zhang, Y.; Chen, J. X.; Wang, T.; Wang, W. X.; Zhao, Y. R.; Fan, X. L.; Chen, C. X.; Xu, H. Rapid Hemostasis Resulting from the Synergism of Self-Assembling Short Peptide and O-Carboxymethyl Chitosan. *ACS Appl. Mater. Interfaces* **2020**, *12*, 55574−55583.
(26) Gelain, F.; Luo, Z. L.; Zhang, S. G. Self-Assembling Peptide EAK16 and RADA16 Nanofiber Scaffold Hydrogel. *Chem. Rev.* **2020**, *120*, 13434−13460.
(27) Yan, J.; He, W.; Yan, S.; Niu, F.; Liu, T.; Ma, B.; Shao, Y.; Yan, Y.; Yang, G.; Lu, W.; Du, Y.; Lei, B.; Ma, P. X. Self-Assembled Peptide-Lanthanide Nanoclusters for Safe Tumor Therapy: Overcoming and Utilizing Biological Barriers to Peptide Drug Delivery. *ACS Nano* **2018**, *12*, 2017−2026.
(28) He, W.; Yan, J.; Jiang, W.; Li, S.; Qu, Y.; Niu, F.; Yan, Y.; Sui, F.; Wang, S.; Zhou, Y.; Jin, L.; Li, Y.; Ji, M.; Ma, P. X.; Liu, M.; Lu, W.; Hou, P. Peptide-Induced Self-Assembly of Therapeutics into a Well-Defined Nanoshell with Tumor-Triggered Shape and Charge Switch. *Chem. Mater.* **2018**, *30*, 7034−7046.
(29) He, W.; Yan, J.; Sui, F.; Wang, S.; Su, X.; Qu, Y.; Yang, Q.; Guo, H.; Ji, M.; Lu, W.; Shao, Y.; Hou, P. Turning a Luffa Protein into a Self-Assembled Biodegradable Nanoplatform for Multitargeted Cancer Therapy. *ACS Nano* **2018**, *12*, 11664−11677.
(30) He, W.; Mazzuca, P.; Yuan, W.; Varney, K.; Bugatti, A.; Cagnotto, A.; Giagulli, C.; Rusnati, M.; Marsico, S.; Diomede, L.; et al. Identification of amino acid residues critical for the B cell growth-promoting activity of HIV-1 matrix protein p17 variants. *Biochim. Biophys. Acta, Gen. Subj.* **2019**, *1863*, 13−24.
(31) Zheng, X.; Yan, J.; You, W.; Li, F.; Diao, J.; He, W.; Yao, Y. De Novo Nano-Erythrocyte Structurally Braced by Biomimetic Au(I)-peptide Skeleton for MDM2/MDMX Predation toward Augmented Pulmonary Adenocarcinoma Immunotherapy. *Small* **2021**, *17*, 2100394.
(32) Yan, S.; Yan, J.; Liu, D.; Li, X.; Kang, Q.; You, W.; Zhang, J.; Wang, L.; Tian, Z.; Lu, W.; et al. A nano-predator of pathological MDMX construct by clearable supramolecular gold (I)-thiol-peptide complexes achieves safe and potent anti-tumor activity. *Theranostics* **2021**, *11*, 6833.
(33) Hou, H.; Wang, S. K.; Zhu, X.; Li, Q. Q.; Fan, Y.; Cheng, D.; Li, B. F. A novel calcium-binding peptide from Antarctic krill protein hydrolysates and identification of binding sites of calcium-peptide complex. *Food Chem.* **2018**, *243*, 389−395.
(34) Moreira Teixeira, L. S.; Feijen, J.; van Blitterswijk, C. A.; Dijkstra, P. J.; Karperien, M. Enzyme-catalyzed crosslinkable hydrogels: Emerging strategies for tissue engineering. *Biomaterials* **2012**, *33*, 1281−1290.
(35) Yan, J.; Yao, Y.; Yan, S.; Gao, R.; Lu, W.; He, W. Chiral Protein Supraparticles for Tumor Suppression and Synergistic Immunotherapy: An Enabling Strategy for Bioactive Supramolecular Chirality Construction. *Nano Lett.* **2020**, *20*, 5844−5852.
(36) She, J.; Li, Y.; Yan, S.; Yan, Y.; Liu, D.; Li, S.; Guo, Y.; Xue, Y.; Yao, Y.; Yan, J.; He, W. De novo supraparticle construction by a self-assembled Janus cyclopeptide to tame hydrophilic microRNA and hydrophobic molecule for anti-tumor cocktail therapy and augmented immunity. *Chem. Eng. J.* **2020**, *401*, 126080.
(37) Yan, J.; Ji, F.; Yan, S.; You, W.; Ma, F.; Li, F.; Huang, Y.; Liu, W.; He, W. A general-purpose Nanohybrid fabricated by Polymeric Au(I)-peptide precursor to wake the function of Peptide Therapeutics. *Theranostics* **2020**, *10*, 8513−8527.
(38) He, W.; Campilongo, F.; Caccuri, F.; Yuan, W.; Varney, K.; Caruso, A.; Gallo, R.; Lu, W. F-103 A conformational switch that turns on the B cell growth-promoting activity of the HIV-1 matrix protein p17. *JAIDS, J. Acquired Immune Defic. Syndr.* **2016**, *71*, 61.

https://doi.org/10.1021/acs.nanolett.1c01800
Nano Lett. XXXX, XXX, XXX−XXX